nature physics

ARTICLES

PUBLISHED ONLINE: 23 JANUARY 2017 | DOI: 10.1038/NPHYS4010

Edge reconstruction in fractional quantum Hall states

Ron Sabo[1†], Itamar Gurman[1†], Amir Rosenblatt[1], Fabien Lafont[1], Daniel Banitt[1], Jinhong Park[2], Moty Heiblum[1*], Yuval Gefen[2], Vladimir Umansky[1] and Diana Mahalu[1]

The nature of edge reconstruction in the quantum Hall effect (QHE) and the issue of where the current flows have been debated for years. Moreover, the recent observation of proliferation of 'upstream' neutral modes in the fractional QHE has raised doubts about the present models of edge channels. Here, we present a new picture of the edge reconstruction in two of the hole-conjugate states. For example, while the present model for $\nu=(2/3)$ consists of a single downstream chiral charge channel with conductance $(2/3)(e^2/h)$ and an upstream neutral mode, we show that the current is carried by two separate downstream chiral edge channels, each with conductance $(1/3)(e^2/h)$. We uncover a novel mechanism of fragmentation of upstream neutral modes into downstream propagating charge modes that induces current fluctuations with zero net current. Our unexpected results underline the need for better understanding of edge reconstruction and energy transport in all fractional QHE states.

It is well accepted that transport of charge in the QHE is mediated by downstream chiral edge channels, while the bulk is incompressible. The Hall conductance exhibits plateaus centred at rational filling factors ν, given by $G_H=\nu(e^2/h)$ (e—electron's charge; h—Planck's constant), accompanied by a vanishing longitudinal conductance (and resistance). Whereas the edge profile of particle-like (Laughlin's) fractional states was expected to mimic that of integer states[1,2], the hole-conjugate states were believed to be more complex. For the latter, substantial 'edge reconstruction' was expected, with added upstream chiral edge modes[3]. A new ground state due to unavoidable inter-channel scattering and interactions is established, with upstream neutral modes joining the downstream charge channels[4–6]. However, the recent observation of upstream chiral neutral modes in particle-like fractions[7,8], accompanied by energy flow through the incompressible bulk, raised doubts as to the validity of the presently accepted edge models.

Here, we studied two hole-conjugate states, $\nu=(2/3)$ (in some detail) and $\nu=(3/5)$. For the former, Girvin and MacDonald proposed[3,9] an edge structure composed of two counter-propagating channels: a downstream chiral channel with conductance (e^2/h) and an upstream chiral channel with conductance $-((1/3)(e^2/h))$ (the minus sign stands for counter-propagating, Fig. 1a, I). With the upstream not observed[10], Kane *et al.*[4,5] (for short, KFP), proposed taking into account inter-channel interactions accompanied with inter-channel scattering—an equilibrated new ground state composed of a downstream charge channel (with conductance $(2/3)(e^2/h)$) and an upstream neutral mode (with zero net electric current, see Fig. 1a, II). Other proposals consisted of either two downstream edge channels, each with conductance $(1/3)(e^2/h)$ (refs 2,11); or two counter-propagating edge channels added to Girvin–MacDonald's model at the sample's edge, yielding an edge composed of (in order from bulk to edge, in units of e^2/h): $-(1/3), 1, -(1/3), (1/3)$ charge channels[12,13]. In that model, depicted in Fig. 1a, III, the inner three edge channels were expected to renormalize to a single downstream charge mode with conductance $(1/3)(e^2/h)$ accompanied by two near-by upstream neutral modes, and an additional downstream charge channel with conductance $(1/3)(e^2/h)$ near the sample's edge.

On the experimental front, recent observations of upstream neutral modes[6,7,14–16] supported the KFP model of the $\nu=(2/3)$ state[5]. However, Bid *et al.*[17], while studying partitioning of the downstream charge channel for $\nu=(2/3)$ in a quantum point contact (QPC), reported a $(1/3)(e^2/h)$ conductance plateau (at QPC transmission $t=(1/2)$) with strong noise. Since shot noise results from stochastic partitioning of a noiseless particle stream, the noise on plateau leads to a discrepancy in our present understanding, and thus triggered our present study.

Figure 1b,c portrays 'two-QPC' configurations; one with $L=9\,\mu$m and the other with $L=0.4\,\mu$m, which are employed to understand this phenomenon. These two versions were fabricated in a high-mobility two-dimensional electron gas (2DEG) embedded in high-mobility GaAs–AlGaAs heterostructures. The proposed description of the chiral edge channels plotted in the figures will be justified below.

The dependence of the total transmission $t_{S1\to D1}$ ($L=9\,\mu$m) on the split-gate voltage V_{QPC2} is plotted in Fig. 2a. Following the '$t_{S1\to D1}=(t_1/2)$ conductance plateau', observed for all values of t_1 once $t_2=(1/2)$, we find it obeys the generalized total transmission $t_{S1\to D1}=t_1\times t_2$. This observation supports a 'single downstream-like' charge mode behaviour. Similar results were obtained for $L=5.3\,\mu$m (not shown). A striking difference is observed with the configuration $L=0.4\,\mu$m (Fig. 2b). Here, the 'conductance plateau' $t_{S1\to D1}=(1/2)$ remains as long as $t_2=(1/2)$ and $t_1\geq(1/2)$ (with $t_{S1\to D1}\sim t_1$ for $t_1<(1/2)$). This is consistent with two independent, spatially separated, unequilibrated downstream charge channels; each with conductance $(1/3)(e^2/h)$. Specifically, for $t_1=t_2=t_{S1\to D1}=(1/2)$ no current arrives at D2 ($t_{S1\to D2}<10^{-3}$; see Supplementary Information). Evidently, these two outcomes suggest that equilibration, via inter-edge charge tunnelling, takes place at a length scale of a few micrometres (namely less than 5.3 μm).

Is the observed edge reconstruction in the $\nu=(2/3)$ state unique to this state? Testing similar 'two-QPC' configurations

[1]Braun Center for Submicron Research, Department of Condensed Matter Physics, Weizmann Institute of Science, Rehovot 76100, Israel. [2]Department of Condensed Matter Physics, Weizmann Institute of Science, Rehovot 76100, Israel. [†]These authors contributed equally to this work.
*e-mail: moty.heiblum@weizmann.ac.il

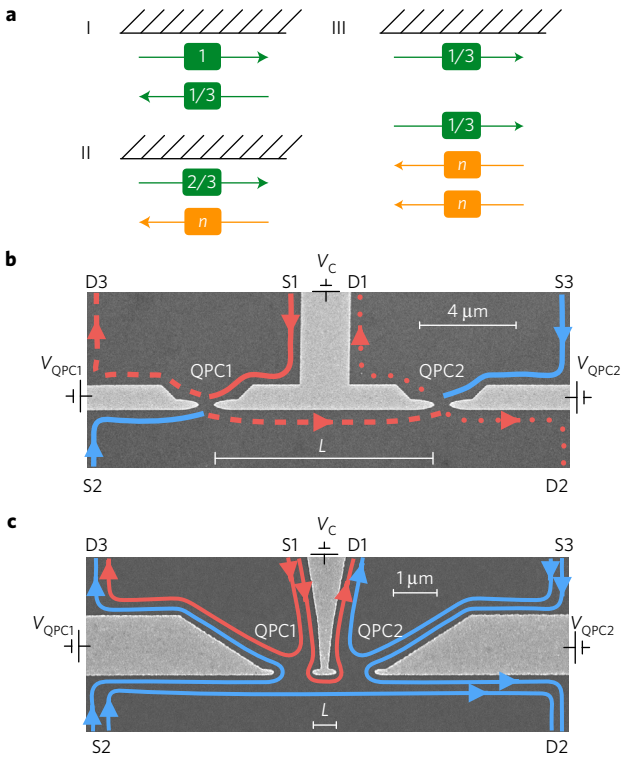

Figure 1 | The different theoretical modes of $\nu = 2/3$ and the observation of two separate charge modes and the way to differentiate between one and two channels. a, Three different theoretical descriptions of the $\nu = (2/3)$ edge structure. I: an upstream charge mode with conductance $(1/3)(e^2/h)$ followed with a downstream charge mode with conductance (e^2/h) (MacDonald picture). II: mixing of the two above-mentioned channels, due to impurity scattering, resulting with a single downstream charge mode and an upstream neutral mode (KFP picture). III: four-edge modes model is obtained by adding two counter-propagating $(1/3)(e^2/h)$ edge modes to I, and then introducing scattering (Meir picture). **b**, A scanning electron microscope (SEM) image of the two consecutive QPCs configuration. Current impinging from S1 (clockwise chirality) can be partitioned at both QPCs, which are controlled by the voltages V_{QPC1}, V_{QPC2} and V_C (the common middle gate), and arrive at either one of the three drains in the system (D1–D3). Similarly, one can source from S2 or S3 and measure the outcome in the various drains. In the case of a single charge mode, the total transmission from S1 to D1 (red edge) is the product of the two transmission processes, specifically once both are tuned to half transmission the total outcome will be one quarter. In addition, the transmission to D2 will also be one quarter. **c**, Similar to **b**, but with two charge modes. In this case the resulting transmission from S1 to D1 is highly dependent on which channel each QPC is tuned to. Specifically, if both QPCs are tuned to half transmission (as illustrated here) it means the two channels are split at each QPC and the overall result will be one half. Furthermore, in this case no net current will arrive at D2.

at $\nu = (3/5)$ resulted in qualitatively similar observations. A single-QPC $(1/3)(e^2/h)$ conductance plateau, corresponding to $t = (5/9)$, was observed (blue line in Fig. 2c,d); also laden with noise. Very much like in $\nu = (2/3)$, the 'two-QPC' configuration with $L = 0.4\,\mu$m proved the presence of unequilibrated channels (Fig. 2d); while in the $L = 5.3\,\mu$m device, full equilibration took place (Fig. 2c). In identical measurements at $\nu = 2$ (two integer edge channels), and at $\nu = 2/5$ (two composite fermion edge channels)[18], the edge channels remained unequilibrated even at $L = 9\,\mu$m (see Supplementary Section 1).

To further probe the inter-edge tunnelling, we fabricated a small electronic Fabry–Perot interferometer (FPI), with an area $400 \times 400\,\text{nm}^2$ defined by two QPCs and modified by charging the plunger gate with V_P (Fig. 3a). Interference of such a small FPI is known to be dominated by Coulomb interactions[19–22].

Operating at filling $\nu = (2/3)$, with the two QPCs strongly pinched ($t_{QPC1}, t_{QPC2} \ll 1$), ubiquitous periodic conductance peaks were observed as function of V_P (Fig. 3b). These peaks are known not to show a magnetic field (B) dependence if the 'interfering' channel is the outermost one (see Supplementary Section 2)[19]. Adhering to the two-channel model, we tuned each QPC to $t_{QPCi} = (1/2)$ (with the two '1/3 channels' sketched in Fig. 3a). Evidently, the total transmission $t_{FPI} = (1/2)(G_{FPI} = (1/3)(e^2/h))$, with the outer '1/3 channel' being fully transmitted. Scanning V_P revealed a series of strong quasi-periodic conductance dips protruding down from $G_{FPI} = (1/3)(e^2/h)$ (Fig. 3c). We ascribe these dips to resonant tunnelling. While the outermost edge channel (red line at bottom and blue line at top, Fig. 3a) is allowed to pass freely through the FPI, the inner channel (white line) is fully confined, and thus quantized. A very small, but finite, tunnelling probability between the outer and inner channels allows resonant tunnelling from the bottom (red) channel to the upper (blue) channel via the inner (white) channel. In other words, every time a quantized state in the confined inner edge channel (white) is aligned with the Fermi energy of the outer edge channel, quasi-particles will backscatter via resonant tunnelling and arrive at D2 instead of D1. Significant conductance dips will be evident at sufficiently low temperatures.

A two-dimensional $V_P - B$ plot of the conductance dips exhibits the familiar Coulomb dominated behaviour of the 'inner dot' (Fig. 3d)[21,22]. The extracted area from the B periodicity, $A = (\phi_0/\Delta B) = 0.11\,\mu\text{m}^2$, is in fair agreement with the lithographic area. Recalling the B independent transmission for the strongly partitioned outermost channel (not shown here), the 'two-channel' model for the $\nu = (2/3)$ is reconfirmed. The temperature dependence of both dips (Fig. 3c) and peaks (Fig. 3b) qualitatively endorses tunnelling of fractionally charged quasi-particles, rather than electrons, between the two edge channels (see Supplementary Section 3).

Although the above results conclusively support the formation of two charge modes, thus challenging the broadly accepted KFP picture, they still do not provide an explanation for the 'noise on the plateau' reported first by Bid and colleagues[17]. We performed noise measurements with the 'two-QPC configuration' at $L = 0.4\,\mu$m (Fig. 1c). Once the two QPCs are tuned to their conductance plateau ($t_1 = t_2 = (1/2)$), current from S1 (red lines) did not arrive at D2; however, significant current fluctuations were measured in D2 (red crosses in Fig. 4a). For comparison, we show the measured excess noise in D2 (blue dots) when $t_1 = 1$ and $t_2 = (1/2)$ (effectively, a single-QPC configuration). The two noise plots, one without net current and the other with, are surprisingly similar.

Similar noise measurements had been repeated for $\nu = 3/5$ state, with the two QPCs tuned to the conductance plateau $(1/3)(e^2/h)$ ($t_1 = t_2 = (5/9)$). Again, strong current fluctuations, with null net current, were observed (see Supplementary Section 6). Note that such current fluctuations are never observed in conductance plateaus of integer or a particle-like fractional states.

In general, stochastic partitioning of an impinging 'quiet current' at a QPC leads to shot noise with spectral density $S = 2qIt\,(1-t)\,\alpha\,(T)$, where q is the partitioned charge, I the impinging d.c. current, t the transmission of the partitioned channel, and $\alpha(T)$ a temperature-dependent reduction factor[23]. It is convenient to define a Fano factor $F = (S/2eIt\,(1-t)\,\alpha\,(T))$, being effectively the partitioned charge, q/e (refs 24–26). When the current fluctuations at the $t = (1/2)$ plateau at the $\nu = (2/3)$ state were analysed, assuming a single charge channel with conductance $(2/3)(e^2/h)$ yielded $F = (2/3)$ at $T \sim 20\,\text{mK}$ and $F = (1/3)$ at higher temperatures ($T \sim 100\,\text{mK}$)[17]. Evidently, this analysis is irrelevant with the presently understood edge reconstruction. Yet,

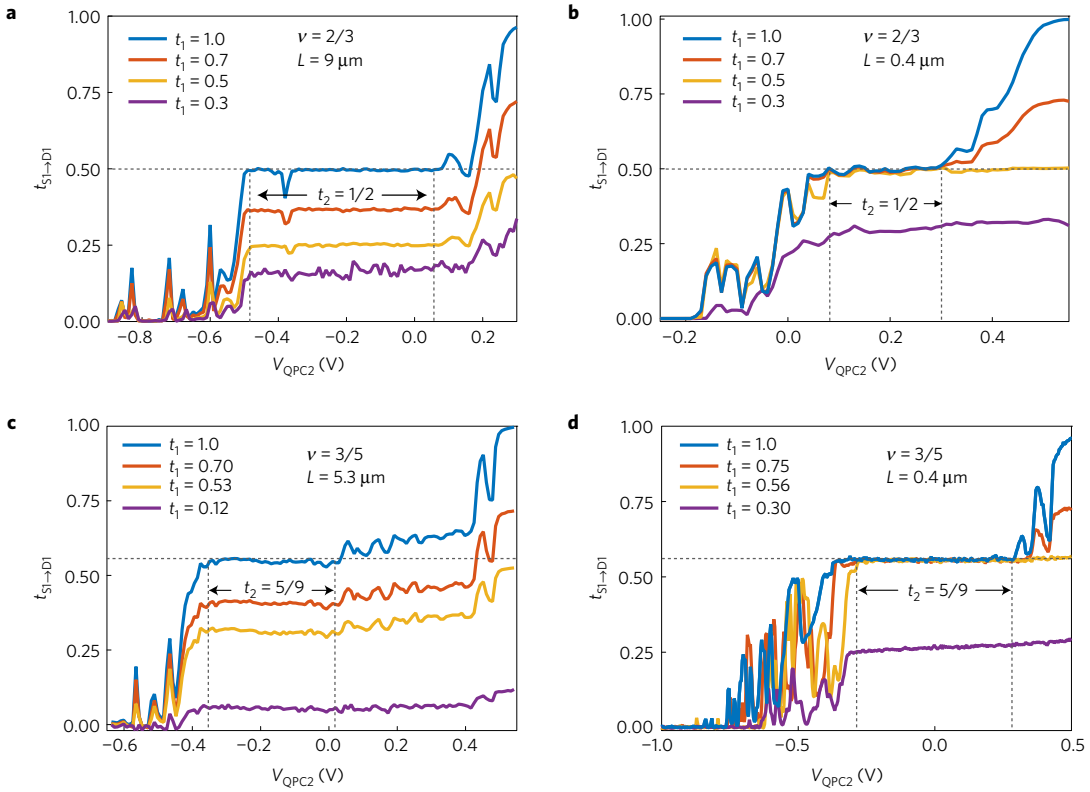

Figure 2 | Comparison between the $L = 9\,\mu m$ and the $L = 0.4\,\mu m$ devices. a, Transmission from S1 to D1 ($t_{S1\to D1}$) as function of V_{QPC2} for different values of t_1 for the $L = 9\,\mu m$ device at $\nu = (2/3)$. The clear plateau at $(t_1/2)$ is a signature of the successive partitioning of a single edge mode. Dashed vertical lines mark the region where QPC2 exhibits a plateau. **b**, Same as **a**, but for the $L = 0.4\,\mu m$ device. The value of the plateau is (1/2) as long as $t_1 > (1/2)$; a signature of transport through two independent edge modes. **c**, $t_{S1\to D1}$ as function of V_{QPC2} for different values of t_1 for a $L = 5.3\,\mu m$ device at $\nu = (3/5)$. The $t_1 = 1$ case (blue curve) shows a transmission plateau of (5/9), which corresponds to an outer channel with $(1/3)\,(e^2/h)$ conductance. Plateaus at different values (proportional to t_1) prove the full equilibration between the two modes. Black dashed line shows the plateau value of (5/9). **d**, Same as **c**, but for the $L = 0.4\,\mu m$ device. The value of the plateau is (5/9) as long as $t_1 \geq (5/9)$, proving that also for $\nu = (3/5)$ the edge is made out of two independent edge modes.

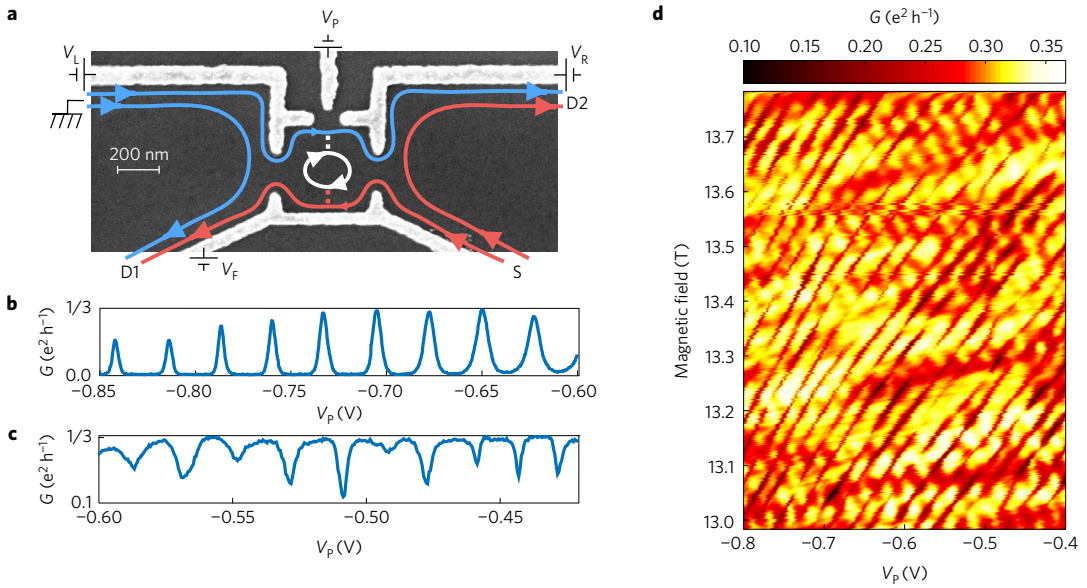

Figure 3 | Fabry–Pérot interferometer (FPI) geometry. a, SEM image of the device together with the edge propagation scheme for the case of $t_{QPC1} = t_{QPC2} = (1/2)$. The outer edge mode, either biased (red) or unbiased (blue), flows unperturbed through both QPCs that define the FPI. The inner edge mode is fully reflected at the QPCs, forming an island inside the FPI (white). Dotted lines denote the tunnelling between the two modes. **b**, Series of conductance (Coulomb blocked) peaks observed for the case of $t_{QPC1}, t_{QPC2} \ll 1$. **c**, Series of quasi-periodic dips below $t_{FPI} = (1/2)$ for the case of $t_{S\to D1}$. These dips are the result of the resonant tunnelling from the lower outer biased channel into the FPI and to the upper unbiased outer channel. **d**, Conductance dips evolution in magnetic field. Equal phase lines have anti-Aharonov–Bohm behaviour, as expected from interference of an inner edge mode. The area extracted from the magnetic field periodicity fits the area of the interferometer.

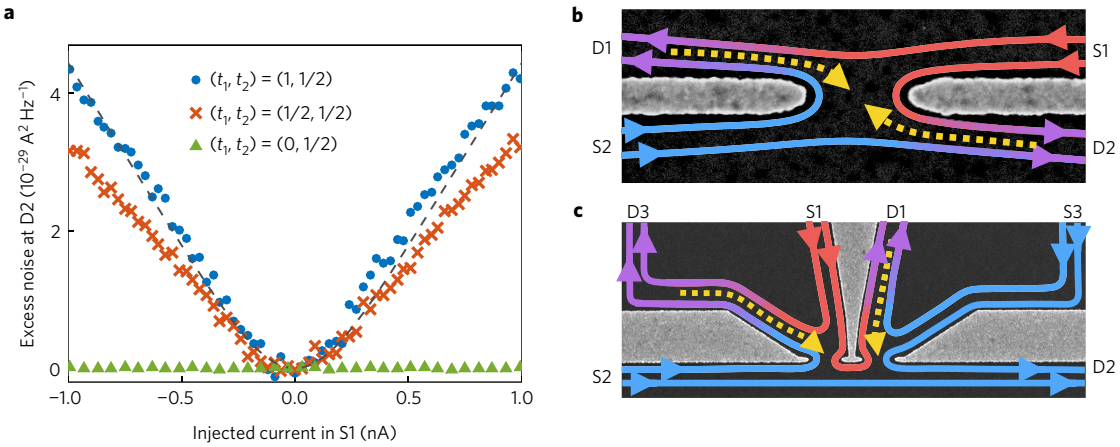

Figure 4 | Finite current fluctuations accompanying null net current, and a schematic model for the interplay between charge and neutral modes. **a**, Current fluctuations measured at D2 as function of current injected at S1 when the QPCs are set to $(t_1, t_2) = ((1/2), (1/2))$ (red crosses) and $(1,(1/2))$ (blue dots). In the latter case, the observed current fluctuations mimic the shot noise predicted when partitioning single charge channel with charge $e^* = (2/3)$ at half transmission and temperature of 20 mK (black dashed line), thus obtaining $F = F_{\rm eff} = 2/3$ (see text). For the $(t_1, t_2) = ((1/2), (1/2))$ configuration (red) we find $F_{\rm eff} = 0.48 \pm 0.05$. As a sanity check, we show null noise once $(t_1, t_2) = (0, (1/2))$ (green triangles), hence QPC1 is completely closed. **b**, Current injected from S1 (red) reached the QPC set to its $t = (1/2)$ plateau together with charge mode at ground potential (blue) emanating from S2. Away from the QPC, two pairs of high and low chemical potential edge channels co-propagate and thus mix (turn purple). This process is accompanied by creation of neutral excitations (yellow), which propagate back upstream towards the QPC. **c**, Same as **b**, but for the two-QPC configuration. Neutral modes are excited only on the way to D1 and D3 flowing back towards the QPCs.

it is convenient to define an 'effective Fano factor', by replacing the $t\,(1-t)$ term with a constant $(1/4)$ and considering I to be the total current leaving the source; namely, $F_{\rm eff} = (2S/eI\alpha(T))$. Note that, whereas for a single QPC $F_{\rm eff} = (2/3)$, in the 'two-QPC' configuration, with $t_1 = t_2 = (1/2)$ (red crosses, Fig. 4a), $F_{\rm eff} \sim (1/2)$.

Sourcing from S3 with $t_1 = t_2 = (1/2)$, led to even more puzzling results. Current carried by the outer (inner) edge channel reached only D2 (D1)—with no current reaching D3. Yet, substantial current fluctuations were measured in D3 with $F_{\rm eff} = 0.40$. Evidently, this currentless-noise must result from upstream neutral mode(s)[14]. Noise measurements in all nine possible configurations, with $t_1 = t_2 = (1/2)$, are summarized in Fig. 5, and compared to predictions based on a simplified theoretical model (see below).

Inspired by the correlation between the noise on plateau and the evident presence of equilibration process between the two 1/3-modes, we propose a new mechanism for the generation of the non-equilibrium noise, proportional to the injected current; due to interplay between counter-propagating charge and neutral modes. Start with a 'hot' (noiseless) current impinging from S1 on a QPC tuned to the $t = (1/2)$ plateau (red lines, Fig. 4b), with a 'cold' current arriving from the grounded S2 (blue lines). Separating the inner and the outer channels at the QPC leads to two co-propagating pairs; 'hot' and 'cold' (moving towards D1 and D2). Since the propagation distance of each pair is tens of micrometres long, equilibration within each pair takes place (purple lines). This process excites upstream neutral modes (dotted lines, yellow), which counter-propagate towards the QPC. These counter-propagating modes fragment into particle–hole pairs in the propagating charge channels. A similar, yet more complicated scenario, with the 'two-QPC' set-up, with current emanating from S1, is shown in Fig. 4c. The remaining question is the observed quantized value of $F_{\rm eff}$.

We now introduce a quantitative model that accounts for the quantized value of $F_{\rm eff}$ in the single-QPC set-up at the $t = (1/2)$ plateau (Fig. 6). Generalization of this model that addresses the different Fano factors in the 'two-QPC' geometry is provided in Supplementary Section 7. The noise-generating mechanism consists of a two-step process (we refer to this as a first hierarchy process): charge equilibration accompanied by generation of neutral mode excitations ('neutralons' or 'anti-neutralons', see

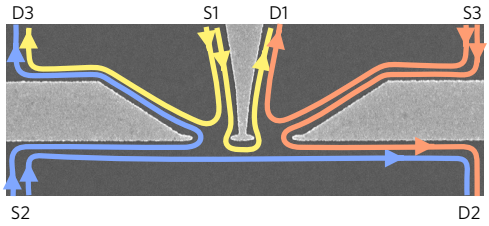

	S1				S2				S3			
	t	$F_{\rm exp}$	$F_{\rm th}^{(1)}$	$F_{\rm th}^{(2)}$	t	$F_{\rm exp}$	$F_{\rm th}^{(1)}$	$F_{\rm th}^{(2)}$	t	$F_{\rm exp}$	$F_{\rm th}^{(1)}$	$F_{\rm th}^{(2)}$
D1	0.5	0.76	2/3	2/3	0.0	0.54	1/3	1/2	0.5	0.51	1/3	1/2
D2	0.0	0.48	1/3	1/2	0.5	0.50	1/3	1/2	0.5	0.66	2/3	2/3
D3	0.5	0.49	1/3	1/2	0.5	0.68	2/3	2/3	0.0	0.40	1/3	1/2

Figure 5 | Effective Fano factors in a two-QPC configuration. Summary of the measured effective Fano factor ($F_{\rm exp}$) and theoretically calculated ones evaluated based on first hierarchy processes ($F_{\rm th}^{(1)}$) and second hierarchy processes ($F_{\rm th}^{(2)}$), in the two-QPC configuration. For convenience, we colour the channels emitted from each source (and their corresponding columns in the table) in different colours—yellow (S1), blue (S2) and red (S3). In each column we present the relative current arriving at each one of the drains (marked as t) and the various effective Fano factors. Notice the accuracy of $F_{\rm exp}$ is ± 0.05.

Supplementary Section 8); and fragmentation (that is, decay) of neutralons, leading to a stochastic creation of quasi-particle/quasi-hole pairs in the charged channels.

The edge of the $\nu = 2/3$ fraction is now expected to support four chiral channels[13]: two downstream charged modes, each with conductance $(1/3)(e^2/h)$, and two inner upstream neutral modes (denoted as yellow lines in Fig. 6), supporting neutralons (and anti-neutralons). Let us assume that during time τ, S1 emits $2N$ quasi-particles (N in each channel), each of charge $e/3$, giving rise to an emitted current $I = (2Ne/3\tau)$. Having the QPC set to the $t = (1/2)$ plateau, one channel is fully reflected while the other is

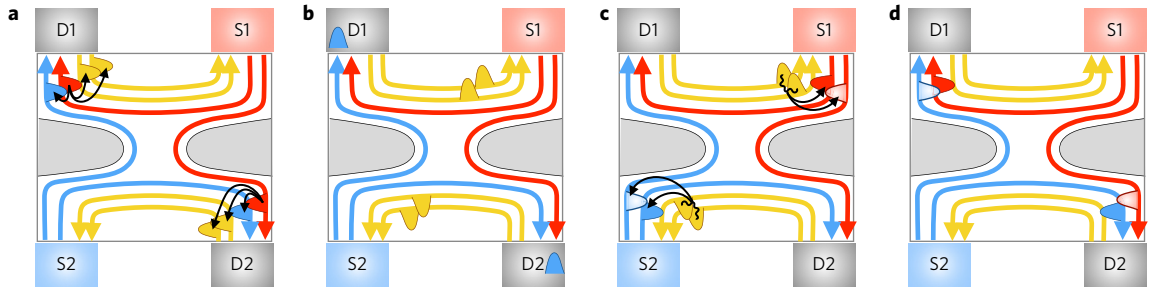

Figure 6 | Neutralon-induced noise. A system tuned to a bulk filling factor $\nu = 2/3$ with a single QPC. The edge consists of four channels—two accommodating downstream charged modes (outer and inner), and two inner upstream neutral modes. The charge channels support quasi-particles (qp) and quasi-holes (qh), possessing a charge of $\pm e/3$. Similarly, the two neutral channels support neutral excitations, dubbed neutralons and denoted as n_1 and n_2. Biased charge channel (emanating from the source S1) are marked in red, unbiased charge channels are in blue and upstream neutral channels in yellow. **a**, Equilibration process involving charge tunnelling and the creation of neutralons, for example $\mathrm{qp}_{\mathrm{outer}} \rightarrow \mathrm{qp}_{\mathrm{inner}} + n_1 + n_2$ (lower right corner) or $\mathrm{qp}_{\mathrm{inner}} \rightarrow \mathrm{qp}_{\mathrm{outer}} + n_1 + n_2$ (upper left corner). A list of all equilibration processes is presented in the Supplementary Information. **b**, The tunnelling qp flow downstream to either drains, while the two excited neutrons flow upstream and fully reflect from the QPC, back towards *S*1 and *S*2. **c**, Each neutralon pair decays to give rise to a qp/qh pair, which is randomly split between the two charge modes. **d**, The excited charge modes flow back to the QPC, the inner one fully reflects and the outer fully transmits, not influencing the average currents at the drains yet contributing to the measured noise (current fluctuations).

fully transmitted. Transmitted (reflected) through (off) the QPC, 'hot' channels (denoted by red solid lines in Fig. 6) are moving in parallel to 'cold' channels emanating from grounded contacts (denoted as blue solid lines). Equilibration between the two channels takes place in both outgoing trajectories (Fig. 6a). Assuming the latter are sufficiently long, complete equilibration implies that $N/2$ quasi-particles tunnel from the 'hot' channel to the 'cold' channel. Close examination of the tunnelling operators reveals that each such tunnelling event is accompanied with the generation of two neutralons (Supplementary Information). Being inner upstream channels, they subsequently fully reflect by the QPC (Fig. 6b). Eventually the neutralons decay through a process that converts a pair of them into a quasi-particle/quasi-hole (quasi-hole/quasi-particle) in the respective (parallel flowing) charge modes (Fig. 6c). These stochastic processes occur with equal probabilities. The newly added quasi-particles and quasi-holes flow towards the QPC where they split—propagating thereafter towards different drains (Fig. 6d). Thus the average current in each charge channel is unchanged by the decay of the neutralons, yet these stochastic processes generate non-equilibrium noise. This noise is proportional to the injected current; hence shot-noise-like.

To characterize this noise quantitatively we introduce $N/2$ random variables a_i (b_i) $i = 1, \ldots, N/2$, referring to the neutralon decay on the lower left (upper right) corner of Fig. 6c. The variables assume the values $+1$ or -1, each with probability $(1/2)$, where $+1$ represents a creation of a quasi-particle in the outer channel and a quasi-hole in the inner channel; while -1 represents the opposite process. The total charge Q_{D1} arriving at D1 during the time interval τ is given by $Q_{\mathrm{D1}} = (e/3)\left(N + \sum_{i=1}^{N/2} a_i - \sum_{i=1}^{N/2} b_i\right)$, with the average charge $\overline{Q_{\mathrm{D1}}} = (e/3)N$, and its variance is $\overline{(\delta Q_{\mathrm{D1}})^2} = \overline{(Q_{\mathrm{D1}} - \overline{Q_{\mathrm{D1}}})^2} = (e^2 N/9)$. Here, we assume that all of the neutralons decay into quasi-particles and quasi-holes. The 'zero frequency' excess noise is $S_{\mathrm{D1}} = 2\lim_{\tau\to\infty}(\overline{(\delta Q_{\mathrm{D1}})^2}/\tau)$, resulting in $F_{\mathrm{eff}} = (2/3)$, in agreement with the experimental value. The same magnitude of noise is measured (and calculated) at D2.

Although this model explains well the quantized value of the noise in a single QPC, when it comes to the 'two-QPC' set-up there are discrepancies between our theory (see $F_{\mathrm{th}}^{(1)}$ in the table at Fig. 5) and the experimentally observed F'_{eff}s (see F_{exp}). These discrepancies may be resolved when second hierarchy processes are included. Consider, for example, the configuration depicted in Fig. 4c, featuring S1 as the biased source (all other contacts are grounded). First hierarchy processes result in a noiseless inner channel and a noisy outer channel (both at same chemical potential) flowing into D2. Yet, local fluctuations in the charge density of the two channels lead to further equilibration processes (facilitating quasi-particle tunnelling from a channel whose instantaneous density, at a given point, is higher than that of the other channel). Such tunnelling processes generate additional neutralons (or anti-neutralons), which flow upstream from D2 to S2. These neutralons annihilate into quasi-particle/quasi-hole pairs at the charge channels, making further contributions to the noise in drains D2 and D3. In a simplified point of view, this process can be understood as equilibrating two channels at different temperatures (as opposed to the first hierarchy process, where the difference was in chemical potential). We refer to this additional two-step process: charge equilibration and decay of neutralons, as a second hierarchy. The consequently revised Fano factors ($F_{\mathrm{th}}^{(2)}$) are displayed in the table (Fig. 5). The second hierarchy process indeed improves the agreement between experiment and theory. For details of the second hierarchy see Supplementary Information.

We portrayed here a thorough experimental and theoretical study of transport in fractional hole-conjugate states. Specifically, in the $\nu = 2/3$ case, we proved that the current is carried by two spatially separated, co-propagating, downstream edge channels (each with conductance $(1/3)(e^2/h)$). Moreover, when these edge channels are out of equilibrium, they equilibrate due to inter-edge tunnelling of fractionally charged quasi-particles, with a typical equilibration length of a few micrometres. Further, we observed unexpected shot-noise-like fluctuations, which we interpret as a unique interplay between charge and neutral modes. Namely, equilibration of charge modes excites neutral modes, which in turn decay and induce noise in the charge modes. In addition, our proposed theoretical model provides a quantitative estimate of the low-temperature Fano factor, which agrees well with the experimental results in the 'single-QPC' set-up, and leads to partial agreement with the noise measured in the 'two-QPC' set-up.

These results suggest a new paradigm with a new approach to looking at fractional states and the behaviour of edge modes, especially in cases where reconstruction at the edge takes place, leading to formation of counter-propagating modes[7]. The yet unresolved discrepancies mentioned in the paper, temperature-dependent Fano factor or inconsistencies in the 'two-QPC' configuration, call for more theoretical and experimental investigations, which will continue to pave the road to a more complete understating of the FQHE.

Methods

Methods, including statements of data availability and any associated accession codes and references, are available in the online version of this paper.

Received 18 May 2016; accepted 9 December 2016; published online 23 January 2017

References

1. Wen, X.-G. Theory of the edge states in fractional quantum Hall effects. *Int. J. Mod. Phys. B* **06,** 1711–1762 (1992).
2. Beenakker, C. W. J. Edge channels for the fractional quantum Hall effect. *Phys. Rev. Lett.* **64,** 216–219 (1990).
3. MacDonald, A. H. Edge states in the fractional quantum Hall effect regime. *Phys. Rev. Lett.* **64,** 220–223 (1990).
4. Kane, C. L., Fisher, M. P. A. & Polchinski, J. Randomness at the edge: theory of quantum Hall transport at filling $\nu = 2/3$. *Phys. Rev. Lett.* **72,** 4129–4132 (1994).
5. Kane, C. L. & Fisher, M. P. A. Impurity scattering and transport of fractional quantum Hall edge states. *Phys. Rev. B* **51,** 13449–13466 (1995).
6. Bid, A. *et al*. Observation of neutral modes in the fractional quantum Hall regime. *Nature* **466,** 585–590 (2010).
7. Inoue, H. *et al*. Proliferation of neutral modes in fractional quantum Hall states. *Nat. Commun.* **5,** 4067 (2014).
8. Altimiras, C. *et al*. Chargeless heat transport in the fractional quantum Hall regime. *Phys. Rev. Lett.* **109,** 026803 (2012).
9. Grivin, S. M. Particle–hole symmetry in the anomalous quantum Hall effect. *Phys. Rev. B* **29,** 6012–6014 (1984).
10. Ashoori, R., Stormer, H., Pfeiffer, L., Baldwin, K. & West, K. Edge magnetoplasmons in the time domain. *Phys. Rev. B* **45,** 3894–3897 (1992).
11. Chang, A. A unified transport theory for the integral and fractional quantum Hall effects: phase boundaries, edge currents, and transmission/reflection probabilities. *Solid State Commun.* **74,** 871–876 (1990).
12. Meir, Y. Composite edge states in the $\nu = 2/3$ fractional quantum Hall regime. *Phys. Rev. Lett.* **72,** 2624–2627 (1994).
13. Wang, J., Meir, Y. & Gefen, Y. Edge reconstruction in the $\nu = 2/3$ fractional quantum Hall state. *Phys. Rev. Lett.* **111,** 246803 (2013).
14. Gross, Y., Dolev, M., Heiblum, M., Umansky, V. & Mahalu, D. Upstream neutral modes in the fractional quantum Hall effect regime: heat waves or coherent dipoles? *Phys. Rev. Lett.* **108,** 226801 (2012).
15. Gurman, I., Sabo, R., Heiblum, M., Umansky, V. & Mahalu, D. Extracting net current from an upstream neutral mode in the fractional quantum Hall regime. *Nat. Commun.* **3,** 1289 (2012).
16. Venkatachalamy, V., Hart, S., Pfeiffer, L., West, K. & Yacoby, A. Local thermometry of neutral modes on the quantum Hall edge. *Nat. Phys.* **8,** 676–681 (2012).
17. Bid, A., Ofek, N., Heiblum, M., Umansky, U. & Mahalu, D. Shot noise and charge at the 2/3 composite fractional quantum Hall state. *Phys. Rev. Lett.* **103,** 236802 (2009).
18. Jain, J. K. *Composite Fermions* (Cambridge Univ. Press, 2007).
19. Ofek, N. *et al*. The role of interactions in an electronic Fabry–Perot interferometer operating in the quantum Hall effect regime. *Proc. Natl Acad. Sci. USA* **107,** 5276–5281 (2010).
20. McClure, D. T., Chang, W., Marcus, C., Pfeiffer, L. N. & West, K. W. Fabry–Perot interferometry with fractional charges. *Phys. Rev. Lett.* **108,** 256804 (2012).
21. Rosenow, B. & Halperin, B. I. Influence of interactions on flux and back-gate period of quantum Hall interferometers. *Phys. Rev. Lett.* **98,** 106801 (2007).
22. Halperin, B., Stern, A., Neder, I. & Rosenow, B. Theory of the Fabry–Pérot quantum Hall interferometer. *Phys. Rev. B* **83,** 155440 (2011).
23. Martin, T. & Landauer, R. Wave-packet approach to noise in multichannel mesoscopic systems. *Phys. Rev. B* **45,** 1742–1755 (1992).
24. de-Picciotto, R. *et al*. Direct observation of a fractional charge. *Nature* **389,** 162–164 (1997).
25. Saminadayar, L., Glattli, D., Jin, Y. & Etienne, B. Observation of the *e*/3 fractionally charged Laughlin quasiparticle. *Phys. Rev. Lett.* **79,** 2526–2529 (1997).
26. Dolev, M., Heiblum, M., Umansky, V., Stern, A. & Mahalu, D. Observation of a quarter of an electron charge at the: $\nu = 5/2$ quantum Hall state. *Nature* **452,** 829–834 (2008).

Acknowledgements

M.H. acknowledges the partial support of the Minerva Foundation, grant no. 711752, the German Israeli Foundation (GIF), grant no. I-1241- 303.10/2014, and the European Research Council under the European Community's Seventh Framework Program (FP7/2007-2013)/ERC Grant agreement No. 339070. Y.G. acknowledges the partial support of DFG Grant No. RO 2247/8-1, the Minerva Foundation, the Russia–Israel IMOS project and by CRC183 of the DFG. I.G. is grateful to the Azrieli Foundation for the award of an Azrieli Fellowship.

Author contributions

R.S., I.G., A.R. and M.H. designed the experiment, R.S., I.G., A.R., F.L., D.B. and M.H. preformed the measurements, R.S., I.G., A.R., F.L. and M.H. did the analysis, J.P. and Y.G. developed the theoretical model. R.S., I.G., A.R., F.L., J.P., M.H. and Y.G. wrote the paper. V.U. grew the 2DEG and D.M. was responsible for the e-beam lithography.

Additional information

Supplementary information is available in the online version of the paper. Reprints and permissions information is available online at www.nature.com/reprints. Correspondence and requests for materials should be addressed to M.H.

Competing financial interests

The authors declare no competing financial interests.

Methods

Sample fabrication. The samples were fabricated in GaAs–AlGaAs heterostructures, embedding a 2DEG, with an areal density of (1.2–2.5) $\times 10^{11}$ cm^{-2} and a 4.2 K 'dark' mobility (3.9–5.1) $\times 10^{6}$ cm^{2} V^{-1} s^{-1}, 70–116 nm below the surface. The different gates were defined with electron beam lithography, followed by deposition of Ti/Au. Ohmic contacts were made from annealed Au/Ge/Ni. The sample was cooled to 20 mK (40 mK for the $\nu = (3/5)$ data) in a dilution refrigerator.

Measurement technique. Conductance measurements were done by applying an a.c. signal with an $\sim 1\,\mu V_{r.m.s.}$ excitation at 700 KHz in the relevant source, which resulted in drain voltage $V_D = I_D R_H$, with R_H, the Hall resistance. The drain voltage was filtered using an LC resonant circuit and amplified by homemade voltage preamplifier (cooled to 1 K) followed by a room-temperature amplifier (NF SA-220F5).

Data availability. The data that support the plots within this paper and other findings of this study are available from the corresponding author upon reasonable request.